

NJC

Accepted Manuscript



This is an *Accepted Manuscript*, which has been through the Royal Society of Chemistry peer review process and has been accepted for publication.

Accepted Manuscripts are published online shortly after acceptance, before technical editing, formatting and proof reading. Using this free service, authors can make their results available to the community, in citable form, before we publish the edited article. We will replace this *Accepted Manuscript* with the edited and formatted *Advance Article* as soon as it is available.

You can find more information about *Accepted Manuscripts* in the [Information for Authors](#).

Please note that technical editing may introduce minor changes to the text and/or graphics, which may alter content. The journal's standard [Terms & Conditions](#) and the [Ethical guidelines](#) still apply. In no event shall the Royal Society of Chemistry be held responsible for any errors or omissions in this *Accepted Manuscript* or any consequences arising from the use of any information it contains.

ARTICLE

Magnetic, Electrochemical and Optical Properties of a Sulfate-bridged Co(II) Imidazole Dimer

Cite this: DOI: 10.1039/x0xx00000x

Michael J. Murphy,^a Pavel M. Usov,^a Felix J. Rizzuto,^a Cameron J. Keper^a and Deanna M. D'Alessandro.*^a

Received 00th January 2012,
Accepted 00th January 2012

DOI: 10.1039/x0xx00000x

www.rsc.org/

The synthesis, as well as the electrochemical, optical and magnetic properties of a sulfate-bridged Co(II) dimer, $[\text{Co}_2(\text{DMIM})_4(\mu_2\text{-O}^2, \text{O}, \text{O}'\text{-SO}_4)_2] \cdot 2\text{MeCN}$ (DMIM = 1,2-dimethylimidazole) (**2**), are reported. The crystal structure consists of two distorted pseudo-octahedral Co(II) centres, each ligated by the μ_2 -(O-O'-sulfato) and μ_2 -(O²-sulfato) bridging modes of the SO_4^{2-} anions. Magnetic studies have identified significant antiferromagnetic coupling between the high spin Co(II) centres, with $J = -28 \text{ cm}^{-1}$. Cyclic voltammetry indicated the presence of a quasi-reversible ligand centred oxidation, while the vis-NIR spectrum of **2** revealed complex splitting of the adsorption bands due to the tetragonal distortion of the octahedral geometry of the Co(II) centres.

Introduction

Polynuclear complexes incorporating paramagnetic metal centres have been extensively investigated for their magnetic, optical and redox properties.¹⁻³ In particular, the magnetic properties of high spin Co(II) dimers are of interest due to the strong orbital angular momentum which, in general, is totally or partially quenched in octahedral environments that are significantly distorted.⁴⁻⁶ The large magnetic anisotropy of these unquenched systems has afforded several single molecule and single chain.^{7,8}

Dinuclear compounds represent the simplest class of materials through which the principles of magnetic exchange coupling and ordering may be elucidated.^{9,10} As such, compiling an index of the relative pairing strengths and influence of bridging ligand exchange pathways is of fundamental interest, as it can be used to interpret the rules for spin alignment and to predict the magnitude of the pairing strength. While $\mu_2\text{-SO}_4^{2-}$ bridged dimers of transition metals have been reported previously, these often include alternative super-exchange pathways that are routed through additional bridging co-ligands, leading to difficulties in isolating the contribution of the sulfate bridge alone.^{11,12}

Herein, we report the crystal structure, spectroscopy and magnetic properties of a sulfate-bridged Co(II) dimer, $[\text{Co}_2(\text{DMIM})_4(\mu_2\text{-O}^2, \text{O}, \text{O}'\text{-SO}_4)_2] \cdot 2\text{MeCN}$ (DMIM = 1,2-dimethylimidazole) (**2**), as well as its precursor $[\text{Co}(\text{DMIM})_4](\text{ClO}_4)_2$ (**1**) (Figure 1). Magnetic studies conducted on **2** indicated significant intra-dimer antiferromagnetic ordering between the $S = 3/2$ Co(II) centres,

arising most prominently from the short Co–O–Co super-exchange pathway.

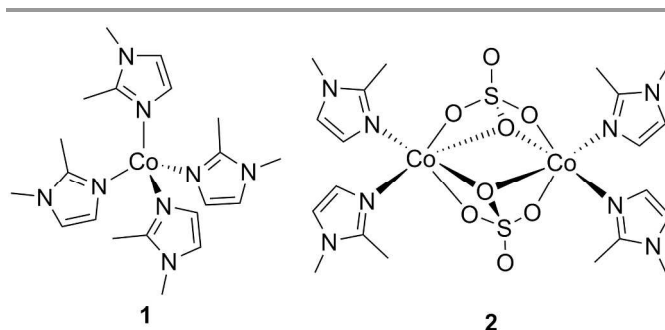


Figure 1. Schematic diagram of $[\text{Co}(\text{DMIM})_4](\text{ClO}_4)_2$ (**1**) and $[\text{Co}_2(\text{DMIM})_4(\mu_2\text{-O}^2, \text{O}, \text{O}'\text{-SO}_4)_2] \cdot 2\text{MeCN}$ (**2**).

Results and Discussion

Synthesis and Structure

We originally began investigating complex **1**, which has been structurally characterised previously and consists of tetrahedral Co(II) centres surrounded by four DMIM ligands,¹³ for its redox activity. Solution-state cyclic voltammetry (CV) measurements (Figure S4) identified one quasi-reversible oxidation process at 1.1 V vs. Fc^0/Fc^+ , which was initially assigned to the Co(II)/Co(III) redox couple. Imidazole analogues, however, also undergo a single oxidation process in a similar potential range to form a radical species.¹⁴ To gain further insight into the electrochemical behaviour of the complex, chemical oxidation using peroxydisulfate was

attempted. Reacting **1** with $[\text{TBA}]_2(\text{S}_2\text{O}_8)$ in acetonitrile caused the purple solution to turn green after one week, potentially indicating that oxidation was successful. Purple plate-like crystals were also recovered from the reaction mixture in moderate yields (*ca.* 60%). Single crystal X-ray diffraction studies (*vide infra*) indicated that the sulfate anions, which originate from the breakdown of peroxydisulfate, had displaced two DMIM ligands from the original Co(II) complex **1**, resulting in a sulfate-bridged Co(II) dimer **2**. Dimer **2** was further investigated for its electrochemical, magnetic and optical properties.

The structure of **2** consists of two equivalent pseudo-octahedral Co(II) centres, each comprising of four O atoms from two equivalent chelating SO_4^{2-} anions, as well as two *cis*-coordinated DMIM ligands (Figure 2). The two Co(II) centres form a dimeric unit as a result of the $\eta^1:\eta^2:\eta^1:\mu_2$ coordination mode of the sulfate anion, with a Co1–Co1 distance of 3.4753(4) Å and a Co1–O1–Co1 angle of 101.03(5)°. Two acetonitrile molecules per dimer were identified as lattice solvent.

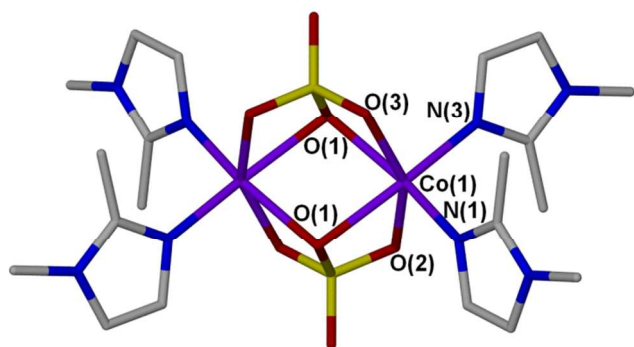


Figure 2. The crystal structure of **2**. Hydrogen atoms and solvent molecules have been omitted for clarity. Co(II) atoms are shown in purple, C in grey, N in blue, O in red and S in yellow.

The distortion of the octahedral geometry of each Co(II) centre is expressed by the compressed O1–Co1–O1 angles of the chelating SO_4^{2-} anions (78.97(5)°), as well as the compacted *trans*-diaxial coordination of the two SO_4^{2-} anions (O2–Co1–O3 angle of 152.62(5)°). Both distorted angles are orientated towards the adjacent Co(II) centre and act to separate the bulkier DMIM ligands (N1–Co1–N3 angle of 98.25(7)°).

Electrochemistry and vis-NIR spectroscopy

Solid-state cyclic voltammetry (CV) was performed on **2** over scan rates in the range 50–200 mV s^{-1} , revealing two oxidation peaks at 0.48 and 1.1 V vs. Fc^0/Fc^+ (Figure 3). The second quasi-reversible oxidation process, originally ascribed to the Co(II)/Co(III) redox couple, was also observed in the anodic sweep of **1** (Figure S4). Due to the differences in coordination geometries between **1** and **2**, the Co(II)/Co(III) redox couple is expected to occur at different potentials. As a result of the similarity in oxidation potentials in **1** and **2**, this process is assigned to the oxidation of the DMIM ligands, which in their

uncoordinated form are known to form free radical species at potentials in this range.¹⁴

The second, less pronounced, irreversible oxidation peak observed at 0.48 V vs. Fc^0/Fc^+ is assigned to the Co(II)/Co(III) couple. This redox wave is broad, indicating that the Co(II) centres oxidise simultaneously.

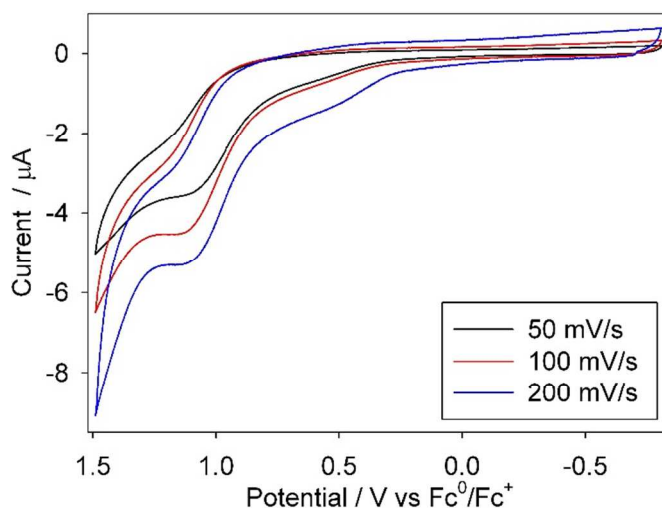


Figure 3. Solid-state CVs of **2** measured at multiple scan rates.

Diffuse reflectance vis-NIR spectra were collected on powdered samples of **1** and **2** (Figure 4). **1** displayed two distinct absorption bands, consistent with its tetrahedral geometry; the bands at 8900 and 17400 cm^{-1} are assigned to ${}^4\text{A}_{2g} \rightarrow {}^4\text{T}_{1g}(\text{F})$ and ${}^4\text{A}_{2g} \rightarrow {}^4\text{T}_{1g}(\text{P})$ transitions, respectively.¹⁵ Both absorption bands are blue shifted relative to the model $[\text{CoCl}_4]^{2-}$ complex due to the larger *d*-orbital splitting contribution of the DMIM ligands.

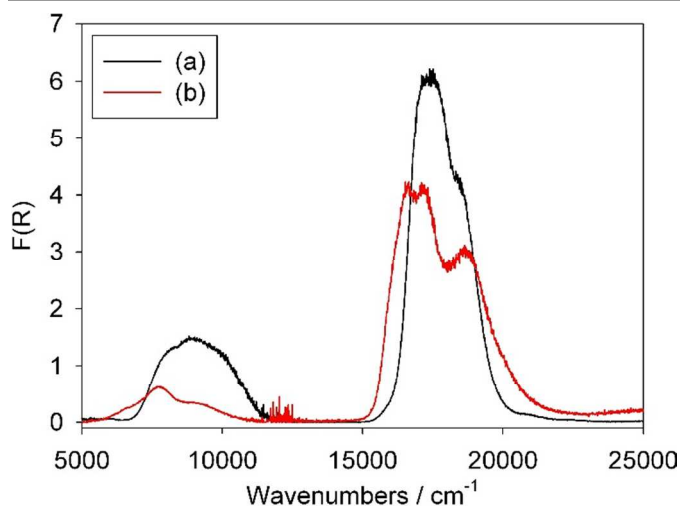


Figure 4. Diffuse reflectance vis-NIR spectra of (a) **1** and (b) **2**.

The spectrum of **2** displayed similar spectroscopic features to its precursor **1**. The band at 7700 cm^{-1} is assigned to the ${}^4\text{T}_{1g}(\text{F}) \rightarrow {}^4\text{T}_{2g}(\text{P})$ transition, while the peaks in the visible region correspond to the ${}^4\text{T}_{1g}(\text{F}) \rightarrow {}^4\text{T}_{1g}(\text{P})$ transition. These transitions are split due to the tetragonal distortion of the octahedral crystal

field and the angular orbital contribution of the metal ions.¹⁶ The characteristic purple colour of **2** arises from the downfield shift of the visible band to lower energy compared to related Co(II) complexes.¹⁷

Magnetic Properties

A polycrystalline sample of the mononuclear Co(II) species **1** exhibited a room temperature $\chi_{\text{M}}T$ of $2.39 \text{ cm}^3 \text{ K mol}^{-1}$ (Figure S5). With spin-orbital coupling largely quenched in the tetrahedral state, significant deviation from the spin-only value is attributed to the anisotropy of the Co(II) ions. With decreasing temperature, $\chi_{\text{M}}T$ is steady until 30 K, at which point it decreases to a local minimum of $1.89 \text{ cm}^3 \text{ K mol}^{-1}$ at 2 K, commensurate with the expected value for a single $S = 3/2$ spin. For mononuclear complexes with anisotropic spins, the temperature dependence of $\chi_{\text{M}}T$ reflects the population of M_s energy levels for the spin ground state. In the case of Co(II), this occurs due to the fluctuation between the $M_s = \pm 3/2$ and $M_s = \pm 1/2$ Kramers doublets. Quantitatively, the energy difference between these states can be measured by the axial zero-field splitting parameter, D . In the present case, this was extracted by the Hamiltonian $\hat{H} = D\hat{S}_z^2 + \beta gS \cdot H$, where \hat{S}_z is the directional spin operator, S is the spin, H is the magnetic field and any transverse anisotropy (E) is ignored. The magnetic susceptibility is therefore an average of the perpendicular magnetic susceptibilities, according to the equations

$$\chi_{\text{M}} = (2\chi_x + \chi_z)/3$$

$$\chi_x = \frac{Ng_x^2\beta^2}{kT} \frac{1 + (3kT/4D)[1 - \exp(-2D/kT)]}{1 + \exp(-2D/kT)}$$

$$\chi_z = \frac{Ng_z^2\beta^2}{4kT} \frac{1 + 9\exp(-2D/kT)}{1 + \exp(-2D/kT)}$$

where the axial g -tensors are described as $g_z \neq g_x = g_y$ and constants have their usual meanings.¹⁰

The best fit to the Hamiltonian produced $g_x = 1.96$, $g_z = 2.85$ and $D = -0.94 \text{ cm}^{-1}$, indicating weak zero-field splitting compared with other tetrahedral mononuclear Co(II) species,^{18,19} and anisotropy of the Co(II) ion in **1**.

Magnetic susceptibility data were also collected on a powdered sample of **2** over the range 2-300 K under an applied field of 1 kOe and are displayed in Figure 5. Initially, it was believed that the distortion of the octahedral symmetry of the Co(II) centres in **2** would be sufficient to quench the orbital moment of the $^4\text{T}_{1g}$ Co(II) ground state; however, the $\chi_{\text{M}}T$ value at 300 K ($6.06 \text{ cm}^3 \text{ K mol}^{-1}$ per Co(II) dimer) is greater than the expected value of $3.75 \text{ cm}^3 \text{ K mol}^{-1}$ for two non-interacting high spin Co(II) centres. This high $\chi_{\text{M}}T$ value is indicative of a substantial orbital contribution to the magnetic susceptibility of **2**. As the ground state retains an orbital angular momentum $L = 1$, a Hamiltonian expressing the spin pairing of two lone $S = 3/2$ centres is not sufficient. Instead, an isotropic Ising model was employed. This model neglects the orbital moving and spin-orbit coupling, treating the Co(II) spins as effective

spins of $S_{\text{eff}} = 1/2$ localised in the ground Kramers doublet. The Hamiltonian is consequently expressed as an effective spin= $1/2$ dimer with a large anisotropy (*i.e.*, $g_{\parallel} \neq g_{\perp}$) and is described by $\hat{H} = 25/9J\hat{S}_A \cdot \hat{S}_B + g_0\beta H_z(\hat{S}_{A,z} + \hat{S}_{B,z})$, where H_z is the field aligned along the z direction, $g_0 = (10/3 + x)$ and other parameters have their usual meanings. In a similar manner to the mononuclear species, the susceptibility is a fractional summation of perpendicular χ values.

$$\chi_{\text{M}} = (\chi_{\parallel} + 2\chi_{\perp})/3$$

$$\chi_{\parallel} = \frac{N\beta^2 g_{\parallel}^2 \exp(25J/18kT)}{2kT \cosh(25J/18kT)}$$

$$\chi_{\perp} = \frac{18N\beta^2 g_{\perp}^2 \tanh(25J/36kT)}{25J}$$

This equation was amended with an uncoupled impurity term to account for the lack of downturn in the graph of χ_{M} vs. temperature. The magnetic susceptibility of **2** is thus described by the equation

$$\chi_{\text{M}} = (1 - p)\chi_{\text{Co(II)}} + p\chi_{\text{para}}$$

where χ_{para} is the Curie Law term,

$$\chi_{\text{para}} = \frac{Ng^2\beta^2 S(S+1)}{3kT}$$

and p is the percentage of Co(II) impurity present.^{10,20}

The best fit of the magnetic data of **2** is shown in Figure 5. Parameters were extracted as $J = -28 \text{ cm}^{-1}$, $g_{\parallel} = 7.19$ and $g_{\perp} = 5.26$, with $p = 0.0254$. While not absolute values (as the equation for χ_{M} provides only an approximation of spin-spin interactions), significant spin-orbit contributions are reflected in the large variances of g from the expected spin-only value of $g = 2$, which qualitatively indicate that the Co(II) anisotropy occurs parallel to the applied field. The difference between parallel and perpendicular g values is reflective of the anisotropy of the Co(II) ions. The negative value of J is consistent with the downturn in $\chi_{\text{M}}T$ with decreasing temperature, indicating that strong antiferromagnetic interactions occur between Co(II) centres within the dimer, presumably through the Co–O–Co bridging motif. Extraction of a negative value for θ after fitting the data to the Curie-Weiss Law further indicated an antiparallel alignment of spins with decreasing temperature: the Weiss constant was $\theta = -37 \text{ K}$ and the Curie constant was $6.80 \text{ cm}^3 \text{ K mol}^{-1}$.

The critical temperature, $T_{\text{N}} = 14.5 \text{ K}$, was determined from the peak of the $d(\chi_{\text{M}}T)/dT$ plot, given the ambiguity in the plot of χ_{M} vs. temperature (due to the presence of a small Co(II) impurity). Inspection of the magnetisation vs. H data (Figure S6) furthermore revealed that the magnetisation under 75 kOe at 2.25 K was only $1.66 \text{ N}\beta$ per Co(II) dimer, far from the saturation value of *ca.* $3 \text{ N}\beta$ expected for a Co(II) ion with $S_{\text{eff}} = 1/2$ and $g \approx 5$.^{21,22} This was taken as further evidence for antiferromagnetic coupling in **2**.

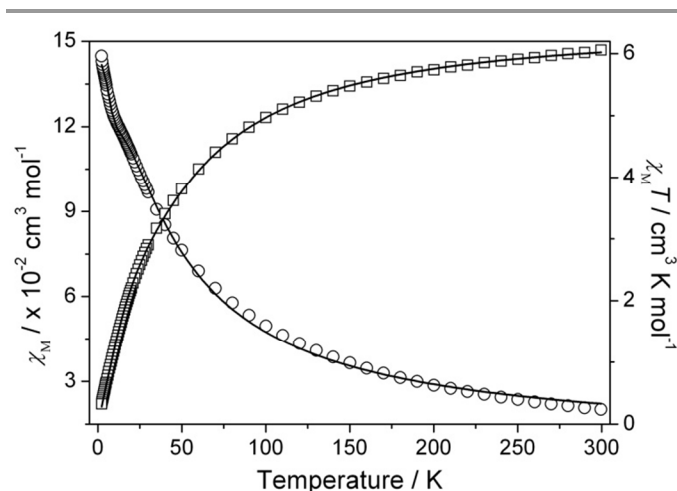


Figure 5. Variable temperature magnetic susceptibility data collected on **2** over the range 2–300 K, plotting χ_M (circles) and $\chi_M T$ (squares) vs. temperature. Black lines are lines of best fit to the data according to the Hamiltonian $\hat{H} = 25/9J\hat{S}_A\hat{S}_B + g_0\beta H_z(\hat{S}_{A,z} + \hat{S}_{B,z})$.

Hence, the distortion of the metal centres in **2** prevents orthogonality between paramagnetic Co(II) and diamagnetic O^{2-} ions. This results in molecular orbitals that overlap out of phase, thus satisfying the criteria for antiferromagnetic coupling, as described by Goodenough^{23,24} and Kanamori.²⁵ With respect to the magnitude of coupling between Co(II) centres, the relatively long Co–O distances (2.245 and 2.258 Å) and secondary superexchange pathways (*i.e.* through the sulfur atom) prevents strong spin pairing between metal centres, which is typically promoted by short connectivities.

While μ_2 - SO_4^{2-} bridged dimers of transition metals have been reported previously, these often include additional super-exchange pathways through multiple bridging co-ligands, leading to uncertainties in the absolute contribution of the sulfate bridge.^{11,12} In **2**, these additional complexities are removed, enabling the direct inference of the coupling across the sulfate bridge to be determined.

Compared to other Co(II) dimers, the antiferromagnetic coupling of **2** is intermediate in strength; it is larger than that of μ_2 -OH₂ dinuclear complexes, while it is weaker than that observed in μ_2 -OAc complexes.²⁶

Conclusions

In summary, we report the structural, electrochemical, spectroscopic and magnetic characterisation of a novel Co(II) dimer **2**, in which Co(II) centres are bridged by the rare $\eta^1:\eta^2:\eta^1:\mu_2$ coordination mode of the sulfate anion.

The electrochemical investigation of **2** revealed a quasi-reversible ligand centred oxidation, as well as a Co(II)/Co(III) redox couple that was absent in its tetrahedral precursor **1**. Splitting of the absorption bands in the electronic spectrum of **2** was observed, reflecting the tetragonal distortion of the octahedral geometry of the Co(II) centres.

Variable temperature magnetic susceptibility measurements conducted on **2** indicated antiferromagnetic coupling of intermediate strength between the distorted high spin Co(II) octahedra, while **1** showed minimal zero field splitting. Significant anisotropy of the high spin Co(II) ions was observed in both **1** and **2**, and characteristic spin-orbit coupling of the $^4T_{1g}$ state was observed in **2**. Quantitatively, the magnetic exchange coupling associated with the two sulfate anion bridges was modelled to be $J = -28 \text{ cm}^{-1}$.

Experimental

Synthetic procedures

[TBA]₂(S₂O₈) was synthesised according to the literature procedure.²⁷

[Co(DMIM)₄(ClO₄)₂ (1). Single crystals of **1** were prepared by a combination of modified literature procedures.¹³ A solution of Co(ClO₄)₂·6H₂O (3.6 g, 10 mmol) in acetonitrile (15 mL) was added dropwise to a solution of DMIM (3.8 g, 40 mmol), forming a purple solution. A purple solid was precipitated by the addition of diethyl ether (100 mL), isolated by vacuum filtration and washed with excess diethyl ether to yield complex **1** (6.1 g, 9.5 mmol, 95% yield based on Co). ESI-MS (ESI⁺, MeCN): *m/z* 221.3, [Co(DMIM)₄]²⁺. Elemental Analysis: Found: C, 37.45; H, 5.0; N, 17.4; Calculated for [Co(DMIM)₄](ClO₄)₂: C, 37.4; H, 5.0; N, 17.5.

[Co₂(DMIM)₄(μ₂-O²⁻, O, O'-SO₄)₂]·2MeCN (2). A solution of **1** (64 mg, 0.10 mmol) in acetonitrile (10 mL) was added to a solution of [TBA]₂(S₂O₈) (0.14 g, 0.20 mmol) in acetonitrile (10 mL). After seven days the purple reaction mixture turned green. A purple precipitate was isolated by vacuum filtration and washed with excess acetonitrile to yield **2** as plate-like purple crystals (25 mg, 0.032 mmol, 65% yield based on **1**). Elemental Analysis: Found: C, 32.0; H, 5.1; N, 14.9; Calculated for [Co₂(DMIM)₄(SO₄)₂]·3H₂O: C, 32.0; H, 5.1; N, 14.85.

Single crystal X-ray diffraction. Measurements on compound **2** were conducted on a Bruker–Nonius FR591 Kappa Apex II diffractometer with Mo–Kα ($\lambda = 0.71073 \text{ \AA}$) radiation at 150 K. Empirical absorption corrections were applied using SADABS.²⁸ Structure solutions were obtained using SHELXS-97²⁹ and refined using SHELXL-97³⁰ in the WinGX interface.³¹ Atoms were refined anisotropically where possible, with the hydrogen atoms refined using a riding-atom model. CCDC 1019336 contains the supplementary crystallographic data for this paper. These data can be obtained free of charge from The Cambridge Crystallographic Data Centre via www.ccdc.cam.ac.uk/data_request/cif.

2 Formula C₂₄H₃₈Co₂N₁₀O₈S₂, $M = 776.62 \text{ g mol}^{-1}$, monoclinic, space group $P2_1/c$ (#14), $a = 10.9888(11)$, $b = 8.6363(9)$, $c = 17.4813(15) \text{ \AA}$, $\beta = 94.688(4)^\circ$, $V = 1653.5(3) \text{ \AA}^3$, $D_{\text{calc}} = 1.560 \text{ g cm}^{-3}$, $Z = 2$, crystal size = $0.120 \times 0.075 \times 0.054 \text{ mm}$, colour = purple, habit = prismatic, temperature = 150(2) K, $\lambda(\text{MoK}\alpha) = 0.71073 \text{ \AA}$, $\mu(\text{MoK}\alpha) = 1.190 \text{ mm}^{-1}$, $2\theta \text{ max} = 52.84^\circ$, $hkl \text{ range} = -13 \text{ to } 13, -10 \text{ to } 10, -21 \text{ to } 21$, $N = 49379$, $N_{\text{ind}} = 3393$ ($R_{\text{merge}} = 0.0342$), $N_{\text{obs}} = 3155$ ($I > 2\sigma(I)$), $N_{\text{var}} = 213$, residuals*

$R_1(F) = 0.0242$, $wR_2(F^2) = 0.1010$, $\text{GoF}(\text{all}) = 1.179$, $\Delta\rho_{\text{min,max}} = -1.046$, $0.651 \text{ e } \text{Å}^{-3}$.

* $R_1 = \frac{\sum ||F_o| - |F_c||}{\sum |F_o|}$ for $F_o > 2\sigma(F_o)$; $wR_2 = \frac{(\sum w(F_o^2 - F_c^2)^2)}{\sum (wF_c^2)^2}^{1/2}$ all reflections

$w = 1/[\sigma^2(F_o^2) + (0.0630P)^2 + 0.8196P]$ where $P = (F_o^2 + 2F_c^2)/3$

Powder X-ray diffraction. Measurements were performed over the $5\text{--}50^\circ 2\theta$ range with a 0.02° step size and 2° min^{-1} scan rate on a PANalytical X'Pert Pro diffractometer fitted with a solid-state PIXcel detector (40 kV, 30 mA, 1° divergence and anti-scatter slits, and 0.3 mm receiver and detector slits) using Cu-K α ($\lambda = 1.5406 \text{ \AA}$) radiation. Profile fits were performed using the Le Bail extraction method in Rietica.³²

Magnetic studies. Magnetic susceptibility measurements were carried out on a Quantum Designs Physical Property Measurement System with a Vibrating Sample Magnetometer attachment. Measurements were collected continuously over the temperature range 2–300 K under a static field of 1 kOe. Variable field measurements were taken over the field range of -75000 to 75000 Oe at 2.25 K .

Vis-NIR spectroscopy. Vis-NIR diffuse reflectance spectra were collected on a Varian CARY 5E UV-Vis-NIR spectrophotometer with a Harrick Omni Diff Probe attachment using Varian WinUV software V3.0. The data were recorded from 5000 to 25000 cm^{-1} with a scan rate of $6000 \text{ cm}^{-1} \text{ min}^{-1}$. Samples were supported on high density filter paper, which was also used to provide the background reference.

Electrochemistry. Electrochemical measurements were performed using a BASi Epsilon Electrochemical Analyser with a standard three-electrode cell. The supporting electrolyte was $0.1 \text{ M } [(n\text{-C}_4\text{H}_9)_4\text{N}]\text{ClO}_4$ in anhydrous acetonitrile (degassed with argon). Cyclic voltammograms (CVs) were recorded using a glassy carbon working electrode (1.0 mm diameter), a Pt wire auxiliary electrode and an Ag wire reference electrode. All potentials are reported against Fc^0/Fc^+ , which was added as an internal reference. For solution-state measurements, *ca.* 1 mg of $[\text{Co}(\text{DMIM})_4](\text{ClO}_4)_2$ (**1**) was dissolved in 3 mL of electrolyte. **2** could not be dissolved in acetonitrile; therefore, CVs were measured on powdered samples which were mechanically immobilised onto the working electrode.

Solid-state Fourier transform infrared spectroscopy. Fourier transform infrared spectra were collected in a potassium bromide (KBr) matrix over the range $4000\text{--}400 \text{ cm}^{-1}$ using a Varian FTS–800 Scimitar series infrared spectrometer. KBr was heated at 400 K under vacuum for 24 h prior to analysis, with $2\text{--}4 \text{ mg}$ of material per 200 mg of KBr used for each measurement. A KBr background was subtracted from the sample scan to obtain a difference spectrum.

Acknowledgements

We gratefully acknowledge support from the Australian Research Council. We also thank Dr Tony Keene for helpful discussions regarding the magnetic data.

Notes and references

^a School of Chemistry, the University of Sydney, NSW, 2006, Australia.

Email: deanna.dalessandro@sydney.edu.au; Fax: +61 (2) 9351-3329
Telephone: +61 (2) 9351-3777

Electronic Supplementary Information (ESI) available: Single crystal and powder X-ray diffraction summaries, FT-IR spectra, cyclic voltammetry and additional magnetic susceptibility plots. See DOI: 10.1039/b000000x/

1. T. D. Keene, D. M. D'Alessandro, K. W. Krämer, J. R. Price, D. J. Price, S. Decurtins and C. J. Kepert, *Inorg. Chem.*, 2012, **51**, 9192-9199.
2. V. Balzani, A. Juris, M. Venturi, S. Campagna and S. Serroni, *Chem. Rev.*, 1996, **96**, 759-834.
3. M. Nakano and H. Oshio, *Chem. Soc. Rev.*, 2011, **40**, 3239-3248.
4. F. Lloret, M. Julve, J. Cano, R. Ruiz-García and E. Pardo, *Inorg. Chim. Acta*, 2008, **361**, 3432-3445.
5. A. Palií, B. Tsukerblat, J. M. Clemente-Juan and E. Coronado, *Int. Rev. Phys. Chem.*, 2010, **29**, 135-230.
6. A. V. Palií, B. S. Tsukerblat, E. Coronado, J. M. Clemente-Juan and J. J. Borrás-Almenar, *Inorg. Chem.*, 2003, **42**, 2455-2458.
7. A. Caneschi, D. Gatteschi, N. Lalioti, C. Sangregorio, R. Sessoli, G. Venturi, A. Vindigni, A. Rettori, M. G. Pini and M. A. Novak, *Angew. Chem. Int. Ed.*, 2001, **40**, 1760-1763.
8. S. Gómez-Coca, A. Urtizberea, E. Cremades, P. J. Alonso, A. Camón, E. Ruiz and F. Luis, *Nature communications*, 2014, **5**.
9. R. Carlin, *Magneto-Chemistry*, Springer-Verlag, 1986.
10. O. Kahn, *Molecular Magnetism*, Wiley-VCH Inc., United States of America, 1993.
11. P. J. van Koningsbruggen, D. Gatteschi, R. A. de Graaff, J. G. Haasnoot, J. Reedijk and C. Zanchini, *Inorg. Chem.*, 1995, **34**, 5175-5182.
12. L. K. Thompson, A. Hanson and B. S. Ramaswamy, *Inorg. Chem.*, 1984, **23**, 2459-2465.
13. E. Bernarducci, P. Bharadwaj, J. Potenza and H. Schugar, *Acta Crystallogr. Sect. C: Cryst. Struct. Commun.*, 1987, **43**, 1511-1514.
14. H. L. Wang, R. M. Omalley and J. E. Fernandez, *Macromolecules*, 1994, **27**, 893-901.
15. J. Ferguson, *J. Chem. Phys.*, 1963, **39**, 116-128.
16. C. J. Ballhausen and C. K. Jorgensen, *Acta Chem. Scand.*, 1955, **9**, 397-404.
17. J. Ferguson, D. L. Wood and K. Knox, *J. Chem. Phys.*, 1963, **39**, 881-889.
18. J. M. Zadrozny, J. Telser and J. R. Long, *Polyhedron*, 2013, **64**, 209-217.
19. A. Buchholz, A. O. Eseola and W. Plass, *Comptes Rendus Chimie*, 2012, **15**, 929-936.
20. M. D. Fryzuk, D. B. Leznoff, R. C. Thompson and S. J. Rettig, *J. Am. Chem. Soc.*, 1998, **120**, 10126-10135.
21. H. L. Sun, B. Q. Ma, S. Gao and G. Su, *Chemical Communications*, 2001, 2586-2587.
22. M. H. Zeng, S. Gao and X. M. Chen, *Inorganic Chemistry Communications*, 2004, **7**, 864-867.
23. J. B. Goodenough, *J. Phys. Chem. Solids*, 1958, **6**, 287-297.
24. J. B. Goodenough, *Physical Review*, 1955, **100**, 564.
25. J. Kanamori, *J. Phys. Chem. Solids*, 1959, **10**, 87-98.

26. S. Ostrovsky, Z. Tomkowicz and W. Haase, *Coord. Chem. Rev.*, 2009, **253**, 2363-2375.
27. S. G. Yang, J. P. Hwang, M. Y. Park, K. Lee and Y. H. Kim, *Tetrahedron*, 2007, **63**, 5184-5188.
28. G. M. Sheldrick, *SADABS. Empirical absorption correction program for area detector data*, University of Göttingen, Germany, 1996.
29. G. M. Sheldrick, *SHELXS-97. Program for crystal structure solution*, University of Göttingen, Germany, 1997.
30. G. M. Sheldrick, *SHELXL-97. Program for crystal structure refinement*, University of Göttingen, Germany, 1997.
31. L. J. Farrugia, *J. Appl. Crystallogr.*, 1999, **32**, 837-838.
32. B. A. Hunter, *IUCR Powder Diffraction*, 1997, **22**, 21.

Electronic Supplementary Information

Magnetic, Electrochemical and Spectroscopic Properties of a Sulfate-bridged Co(II) Imidazole Dimer

Michael J. Murphy,^a Pavel M. Usov,^a Felix J. Rizzuto,^a Cameron J. Kepert^a and Deanna M. D'Alessandro^{*a}

Table S1. Single crystal X-ray diffraction collection summary for **2**.

Compound	2
Formula of the Refinement Model	C ₂₄ H ₃₈ Co ₂ N ₁₀ O ₈ S ₂
Molecular Weight	776.62
Crystal System	monoclinic
Space Group	<i>P2</i> ₁ / <i>c</i> (#14)
<i>a</i> / Å	10.9888(11)
<i>b</i> / Å	8.6363(9)
<i>c</i> / Å	17.4813(15)
<i>β</i> / °	94.688(4)°
<i>V</i> / Å ³	1653.5(3)
<i>D</i> _c / g cm ⁻³	1.560
<i>Z</i>	2
Crystal size / mm	0.120 x 0.075 x 0.054
Crystal colour	purple
Crystal habit	prismatic
Temperature / K	150(2)
<i>λ</i> (Mo-K _α) / Å	0.71073
<i>μ</i> (Mo-K _α) / mm ⁻¹	1.190
<i>T</i> (SADABS) _{min,max}	0.925, 1.0
2θ _{max} / °	52.84
<i>hkl</i> range	-13 to 13, -10 to 10, -21 to 21
<i>N</i>	49379
<i>N</i> _{ind}	3393 (<i>R</i> _{merge} 0.0342)
<i>N</i> _{obs}	3155 (<i>I</i> > 2σ(<i>I</i>))
<i>N</i> _{var}	213
Residuals* <i>R1</i>(<i>F</i>), <i>wR2</i>(<i>F</i>²)	0.0242, 0.1010
GoF(all)	1.179
Residual Extrema / e Å⁻³	-1.046, 0.651

* $R1 = \frac{\sum ||F_o| - |F_c||}{\sum |F_o|}$ for $F_o > 2\sigma(F_o)$; $wR2 = \frac{(\sum w(F_o^2 - F_c^2)^2 / \sum (wF_c^2)^2)^{1/2}}{\sum |F_o|}$ all reflections. $w = 1 / [\sigma^2(F_o^2) + (0.0630P)^2 + 0.8196P]$ where $P = (F_o^2 + 2F_c^2) / 3$

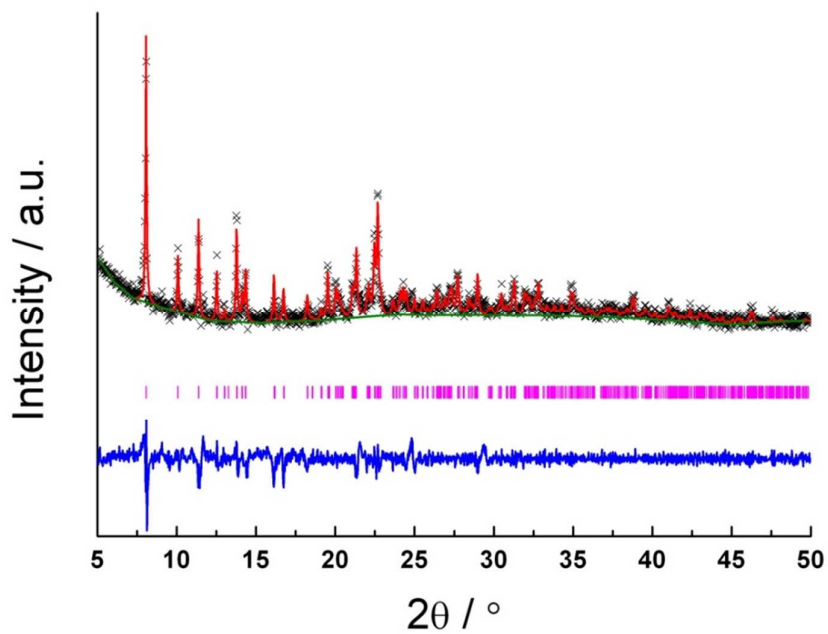


Figure S1. Le Bail fit of **2**: $a = 11.025(4)$, $b = 8.698(2)$, $c = 17.677(5)$ Å, $\beta = 93.29(3)^\circ$ and $V = 1692.4(8)$ Å³.

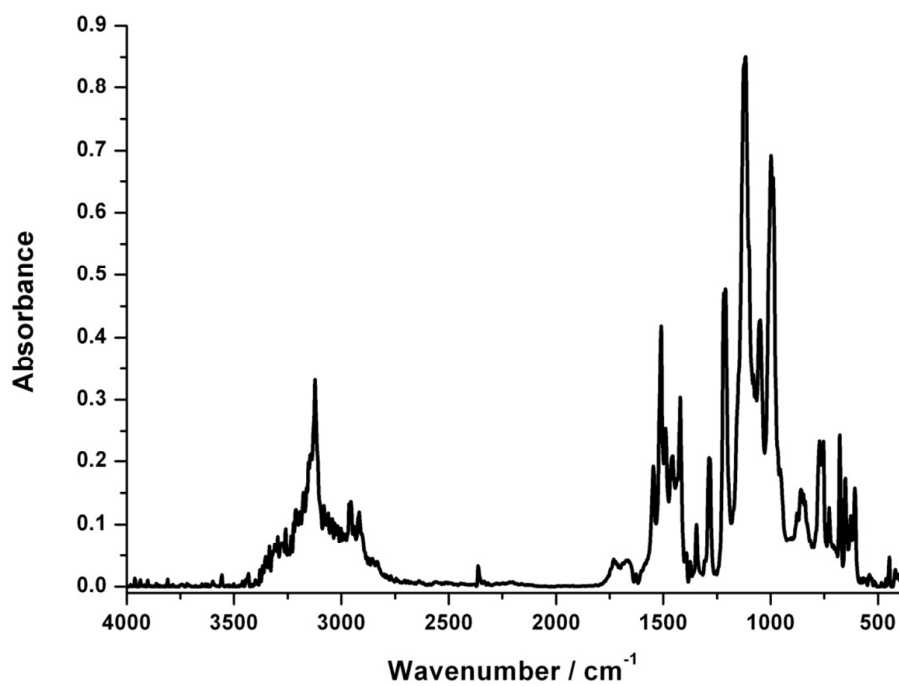


Figure S2. FT-IR spectrum of **2**.

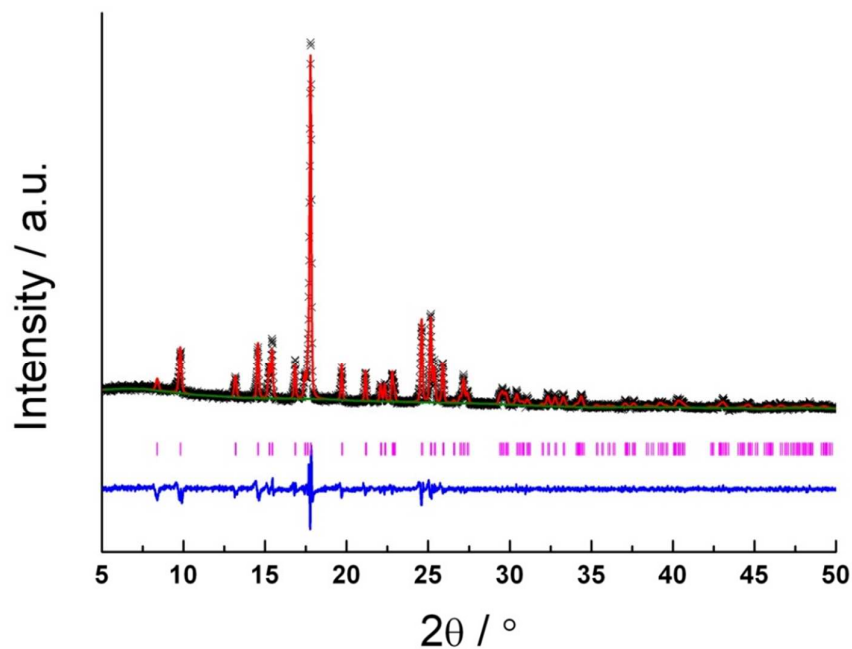


Figure S3. Le Bail fit of **1**: Space group $P3_221$ (#154), $a = b = 12.1377(9)$, $c = 17.393(2)$ Å and $V = 2219.1(3)$ Å³.

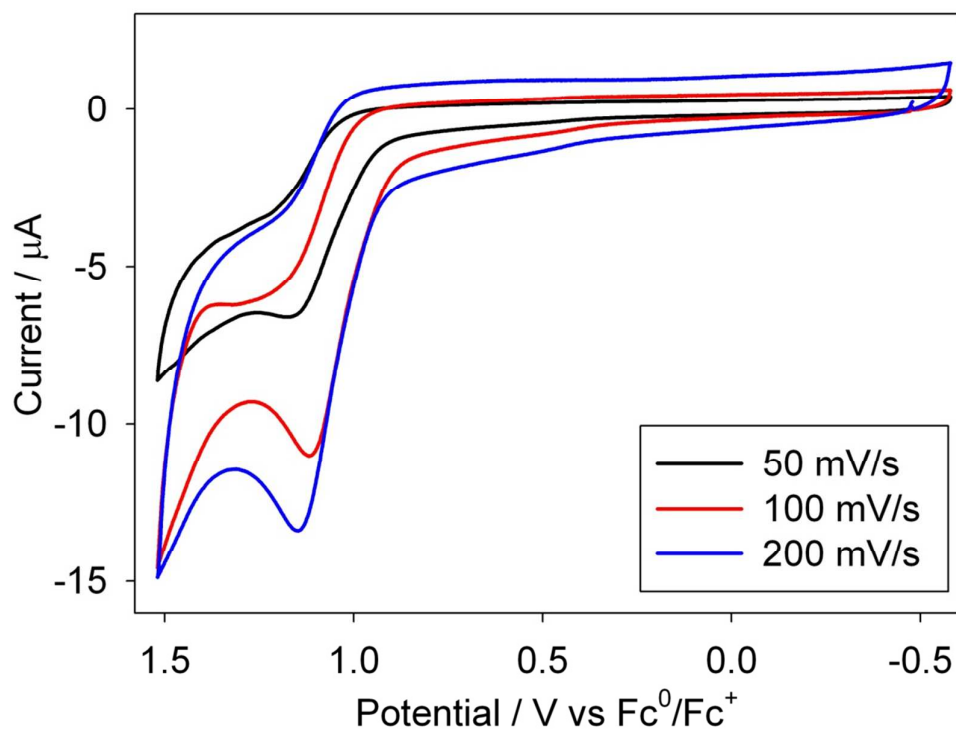


Figure S4. Solution-state cyclic voltammograms of **1** measured at different scan rates.

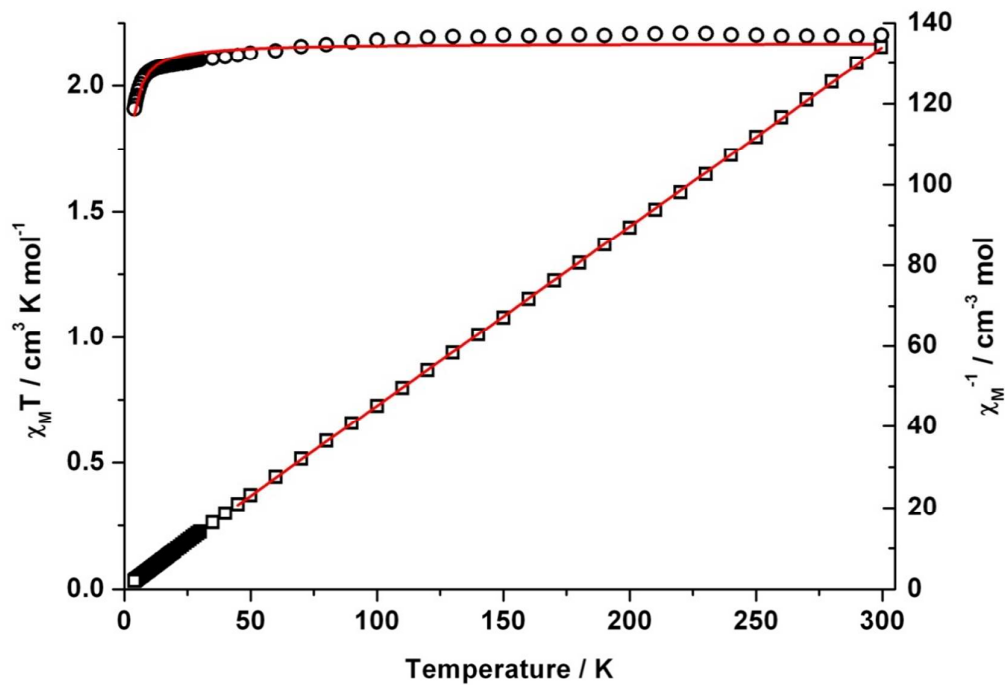


Figure S5. $\chi_M T$ (open circles) and χ_M^{-1} (open squares) vs. temperature plots of **1**. Best fits to the Heisenberg Hamiltonian and Curie-Weiss Law are shown as red lines.

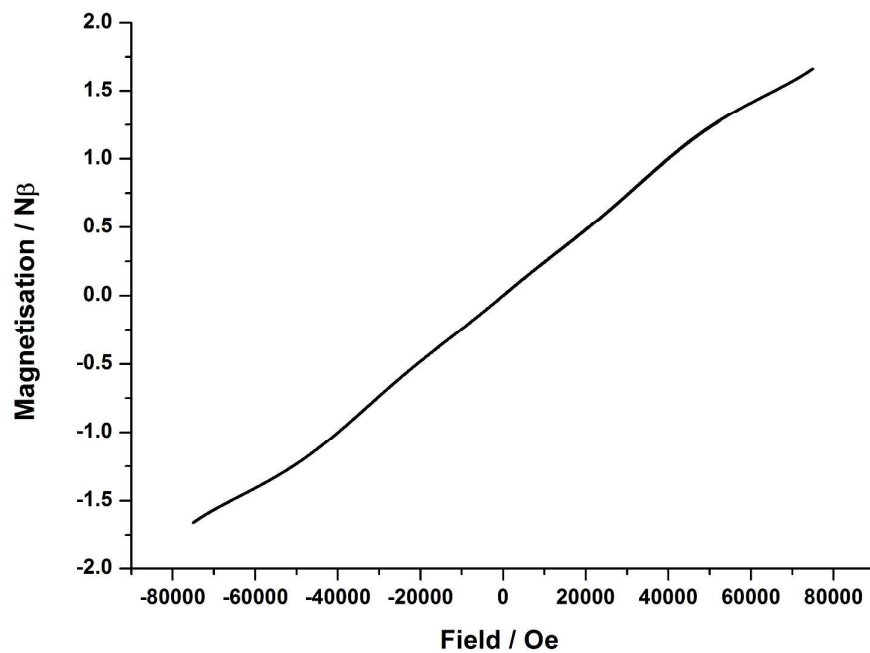


Figure S6. Magnetisation vs. field curve of **2** at 2.25 K.

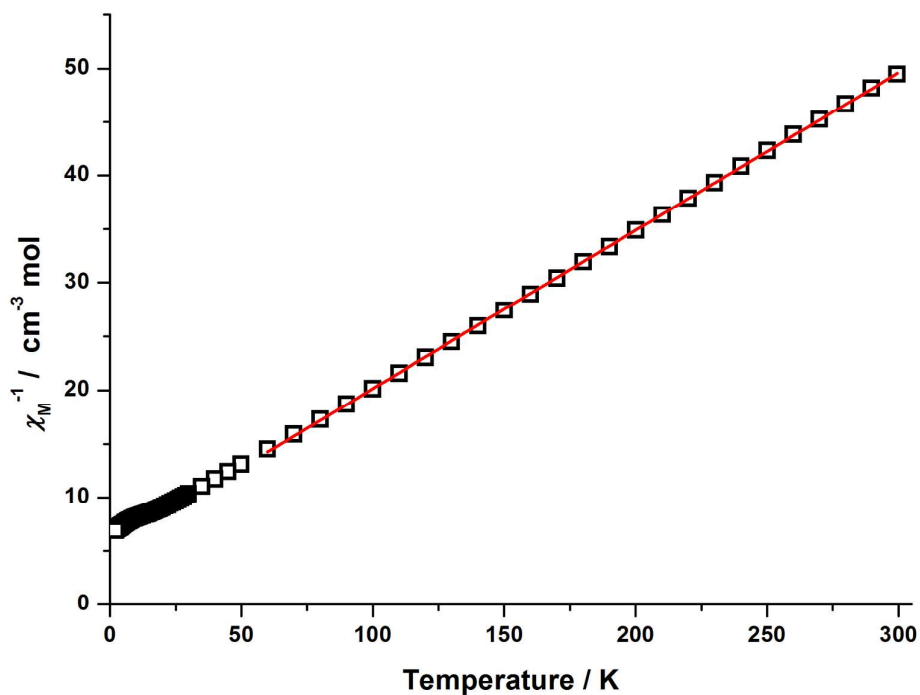


Figure S7. Plot of χ^{-1} vs. temperature for **2**. Red line is the best fit to the Curie Weiss Law.

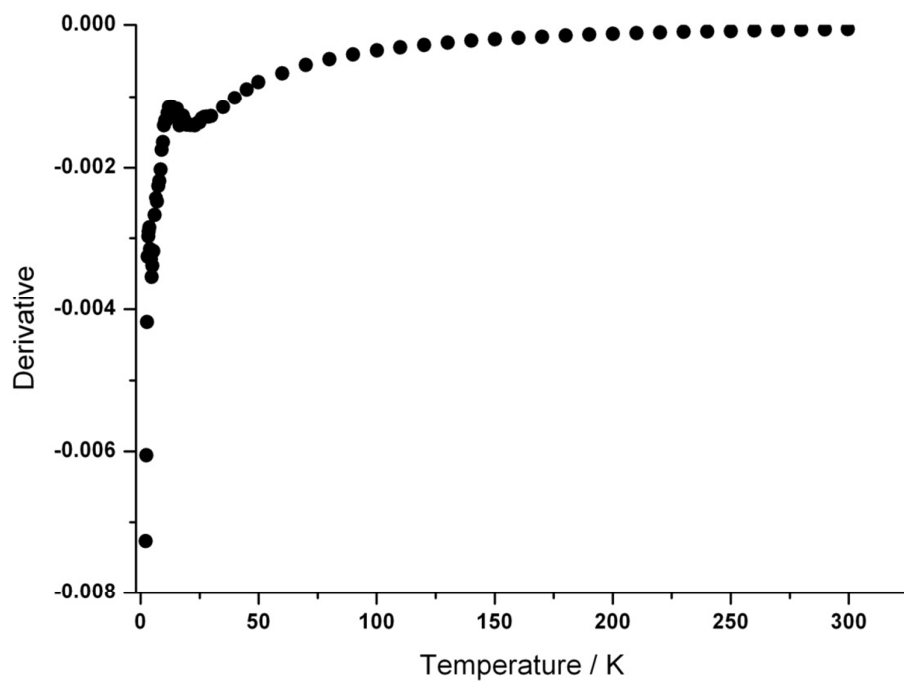
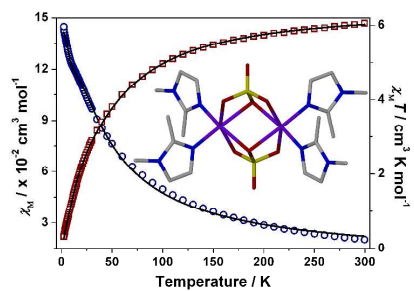


Figure S8. 1st derivative ($d\chi/dT$) of magnetic susceptibility of **2**, indicating the $T_N = 14.5$ K.

Graphical Abstract



The electrochemical, optical and magnetic properties of a sulfate-bridged high spin Co(II) dimer, $[\text{Co}_2(\text{DMIM})_4(\mu_2\text{-O}^2, \text{O}'\text{-SO}_4)_2] \cdot 2\text{MeCN}$ are reported. Antiferromagnetic coupling across the $\mu_2\text{-(O}^2\text{-sulfato)}$ bridging mode has been identified with $J = -28 \text{ cm}^{-1}$.